(4)

TECHNICAL REPORT NO. 11

TO

The Office of Naval Research
Contract No. N00014-86-K-0381

ON SPECIMEN SHAPE EFFECTS AND THE DUCTILITY OF POROUS METALS

A. Geltmacher and D. A. Koss

Department of Materials Science and Engineering
The Pennsylvania State University
University Park, PA 16802

SECURITY CLASSIFICATION OF THIS PAGE

REPORT DOCUMENTATION PAGE

1a. REPORT SECURITY CLASSIFICATION	1b. RESTRICTIVE MARKINGS
2a. SECURITY CLASSIFICATION AUTHORITY	3. DISTRIBUTION/AVAILABILITY OF REPORT
2b. DECLASSIFICATION/DOWNGRADING SCHEDULE	
4. PERFORMING ORGANIZATION REPORT NUMBER(S) Technical Report No. 11	5. MONITORING ORGANIZATION REPORT NUMBER(S) Contract # N00014-86-K-0381
6a. NAME OF PERFORMING ORGANIZATION Department of Mat. Sci. & Eng. The Penn State University 6b. OFFICE SYMBOL (If applicable)	7a. NAME OF MONITORING ORGANIZATION
6c. ADDRESS (City, State and ZIP Code) University Park, PA 16802	7b. ADDRESS (City, State and ZIP Code)
8a. NAME OF FUNDING/SPONSORING ORGANIZATION Office of Naval Research 8b. OFFICE SYMBOL (If applicable)	9. PROCUREMENT INSTRUMENT IDENTIFICATION NUMBER
8c. ADDRESS (City, State and ZIP Code) 800 N. Quincy St. Arlington, VA 22217	10. SOURCE OF FUNDING NOS. PROGRAM ELEMENT NO. / PROJECT NO. / TASK NO. / WORK UNIT NO.
11. TITLE (Include Security Classification) On Specimen Shape Effects on the Ductility of Porous Metals	
12. PERSONAL AUTHOR(S) A. Geltmacher and D. A. Koss	
13a. TYPE OF REPORT 13b. TIME COVERED FROM _____ TO _____	14. DATE OF REPORT (Yr., Mo., Day) February, 1989 15. PAGE COUNT 22
16. SUPPLEMENTARY NOTATION	
17. COSATI CODES FIELD / GROUP / SUB. GR.	18. SUBJECT TERMS (Continue on reverse if necessary and identify by block number)

19. ABSTRACT (Continue on reverse if necessary and identify by block number)

The influence of specimen shape on the elongation to failure has been simulated for materials containing random distributions of pores or voids. The analysis is performed utilizing a computer simulation in which distributions of pores are modeled in two dimensions as arrays of circular holes with differing hole "microstructures". The simulations predict that long, narrow specimens with high aspect ratios should exhibit a loss of ductility which is most pronounced at low area fractions of voids/pores, and when the void/pore distributions exhibit a high degree of clustering. Under these conditions, the ductility data also exhibit considerable scatter. The results, which may be qualitatively understood in terms of imperfection theory, which also contains implications with regard to porosity and fracture toughness at low temperatures.

20. DISTRIBUTION/AVAILABILITY OF ABSTRACT UNCLASSIFIED/UNLIMITED ☐ SAME AS RPT ☐ DTIC USERS ☐	21 ABSTRACT SECURITY CLASSIFICATION
22a. NAME OF RESPONSIBLE INDIVIDUAL	22b. TELEPHONE NUMBER (Include Area Code) 22c. OFFICE SYMBOL

DD FORM 1473, 83 APR EDITION OF 1 JAN 73 IS OBSOLETE.

SECURITY CLASSIFICATION OF THIS PAGE

On Specimen Shape Effects and the Ductility of Porous Metals

A. Geltmacher and D. A. Koss
Department of Materials Science and Engineering
The Pennsylvania State University
University Park, PA 16802

ABSTRACT

The influence of specimen shape on the elongation to failure has been simulated for materials containing random distributions of pores or voids. The analysis is performed utilizing a computer simulation in which distributions of pores are modeled in two dimensions as arrays of circular holes with differing hole "microstructures". The simulations predict that long, narrow specimens with high aspect ratios should exhibit a loss of ductility which is most pronounced at low area fractions of voids/pores, and when the void/pore distributions exhibit a high degree of clustering. Under these conditions, the ductility data also exhibit considerable scatter. The results, which may be qualitatively understood in terms of imperfection theory, also contains implications with regard to porosity and fracture toughness at low temperatures.

INTRODUCTION

The effects of specimen geometry on certain mechanical properties is well known. For example, in the case of the brittle fracture of fibers, the influence of fiber diameter on the fracture strength of long, brittle fibers can be related to the statistical probability of a flaw of critical size.(1) By the same token, high cycle fatigue of porous metals may be specimen-size dependent because of the increased probability of a crack initiation site in a specimen with a larger cross section area.(2) Both of these examples relate to the probability of a critical initial flaw existing in a specimen of given dimensions. Low temperature ductile fracture of metals containing porosity involves the sequential stages of strain induced pore growth and pore linking. Thus in contrast to brittle fracture or high

cycle fatigue, large populations of pre-existing pores are typically involved in the ductile fracture process, and the concept of a single, initial critical flaw usually does not apply in the conventional sense. The purpose of this communication is to utilize a computer simulation in order to explore the influence of specimen shape on the low temperature ductility of metals containing distributions of pre-existing pores. As will be described below, the simulation utilizes a simplified two-dimensional modeling scheme in which three-dimensional arrays of pores are simulated in two dimensions as equisized, cylindrical holes. However, even in its present form, the simulation accurately predicts the step-wise pore linking process during failure[3] and experimentally observed fracture strain values.[3,4] This, plus the consistency of the present predictions with imperfection theory, strongly suggests that this analysis correctly identifies the general trends of specimen-shape effects on the low temperature ductility of porous metals.

BACKGROUND

The present analysis depends on a simulation of void/pore linking during low temperature ductile fracture performed by Magnusen, Srolovitz, and Koss (MSK).[5] That study is based on a simulation of the process of strain-induced pore linking which consists of the following sequence of four stages:[3]

First, local strain gradients develop near individual pores at small macroscopic strains;

Second, upon further straining, failure of ligaments between closely spaced pores occurs due to flow localization. An elongated cavity is created by the ligament failure; due to its eccentric shape, this cavity further localizes flow along its major axis;

Third, successive linking to additional pores occurs in a manner which is controlled by the spatial distribution of pores adjacent to those which have linked. Pore clustering is especially important in this stage as repeated linking results in increased strain concentration;

Fourth, the final stage of pore linking is triggered when a sufficient number of pores have linked to create an imperfection-initiated macroscopic flow instability or crack-like defect. Again pore clustering is important as the generation of large local strains occur and the percolation of the linking by a "void sheet" mechanism can occur.

In the MSK study,[5] the step-wise process of pore linking was simulated utilizing a two-dimensional modeling scheme in which three-dimensional pores are modeled in two dimensions as arrays of equisized, cylindrical holes characterized by an area fraction, hole size, and a minimum interhole spacing. Utilizing experimentally determined strain distributions near holes and critical thickness strain criterion for the failure of ligaments between holes under plane stress conditions, the simulation depicts the sequential stages of void/pore linking. It also accurately predicts the experimentally determined fracture strains of sheet specimens containing random arrays of holes. The good agreement, which will be further demonstrated in this study, was obtained using only empirically represented experimental data and without the use of adjustable parameters to obtain good agreement between the simulation predictions and experimentally determined fracture strain data. The success of the MSK simulation indicates that it is a reasonable basis for extending its range to, for example, the question of specimen shape effects and ductile fracture of materials containing pre-existing porosity.

In both the MSK study and this one, the simulation simplifies a complex, three-dimensional pore linking process by a two-dimensional analog. This is necessary at the present time since the analysis of a three-dimensional pore array with a distribution of pore sizes and shapes would be extremely difficult, computationally intensive and expensive, and probably lack much predictive capability. Despite its simplicity, the MSK simulation requires the same type of input as a general, three-dimensional analysis: specifically, (1) a description of local strain gradients which develop near holes or pores both prior to and after hole/pore linking [these localized strains must be described in terms of the applied macroscopic strain]; (2) a criterion for ligament failure during hole/void linking [which conveniently is a critical thickness strain criterion for the plane-stress case of through-thickness holes in sheet specimens]; and (3) a method of describing the microstructure of the holes/pores in terms of interhole/pore spacings. Three-dimensional solutions to (1) and (2) are especially difficult, and thus the present analysis utilizes the two-dimensional MSK

simulation. Another simplification of the present analysis is the assumption of plane stress conditions, such as in sheets containing holes. Experimental data for specimens containing holes and deforming in either plane stress or predominantly plane strain indicate similar trends of hole/void linking and fracture behavior.[3] Thus, while the magnitudes of the predicted effects will differ between a rigorous three-dimensional analysis and the present one, the methodology, the trends predicted, and the framework of the imperfection analysis as developed in two dimensions should be valid for a three-dimensional porous metal.

RESULTS AND DISCUSSION

A. Basis for the Analysis

The present analysis is based on utilizing the MSK simulation to predict the ductility behavior of specimens possessing the geometries shown in Fig. 1. All three specimens geometries have identical gage section areas of 3225 mm^2 but, as shown in Fig. 1, their length-to-width ratios vary from 1:1 to 20:1. In all cases, the specimens are simulated to deform under plane stress conditions and to contain arrays of through-thickness circular holes either 1.2 or 2.0 mm in diameter, minimum interhole spacing whose values vary from 0.5 to 4.5 mm and with area fractions of holes which range from 0.01 to 0.10. For each case, a minimum of ten computer runs were performed in order to obtain statistically reliable predictions. In order to determine the influence of matrix strain hardening, the simulation examines the contrasting behavior of specimens whose stress-strain behavior corresponds to that of 1100-0 Aluminum (n=0.27) and 70-30 brass (n=0.46).* As is discussed elsewhere,[3,4] increases in the strain hardening capacity of the material has a strong influence on the ability of the material to avoid flow localization between pores and to delay strain-induced pore linking. Strain-rate hardening is also very effective in diffusing deformation. In this study, strain-rate hardening effects are not explicitly

* In this case, the strain hardening exponent n is related to true stress σ and the true strain ε behavior of the material by $n = d\ln\sigma/d\ln\varepsilon$.

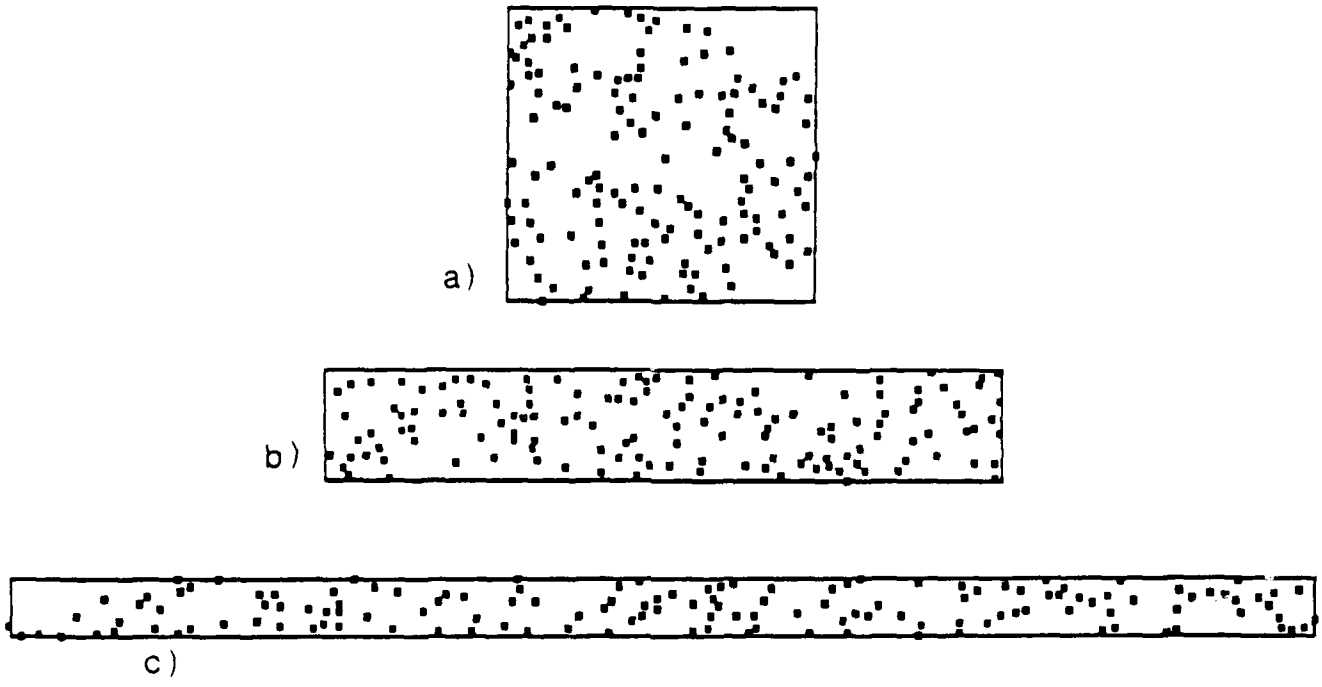

Fig. 1 Scaled examples of random hole arrays containing 0.05 area fraction of 1.2 mm diameter holes with minimum allowable hole spacings of 0.5 mm and length-to-width ratios of (a) 1:1, (b) 5:1 and (c) 20:1. The tensile axis is horizontal.

included in the analysis. Thus the predicted effects are necessarily limited to flow conditions in which strain hardening is the dominant form of slip-induced hardening; this usually implies low temperature deformation and fracture.

As mentioned previously, The MSK simulation is based on (a) the experimentally determined strain gradients near single holes, pairs of unlinked holes, and pairs of linked holes, (b) a critical thickness strain criterion for hole linking in the plane stress (sheet specimen) case, and (c) hole "microstructures" as described by hole size, area fraction, and minimum interhole spacing. It is worth noting that a significant aspect of the simulation is the characteristics of the hole array or hole microstructures, item (c) above. In particular, as depicted in Fig. 2, the minimum interhole spacing parameter S controls the uniformity of hole spacing or the degree of hole clustering. Thus a small value of S results in a considerable clustering of the holes as seen in Fig. 2a, where as Fig 2b, which represents a larger value of S, shows a more uniform distribution of the holes. The tendency of hole/pores to cluster has a significant effect on strain-induced fracture[3,4] and, as will be discussed below, on the predicted specimen-geometry effects.

B. Simulation Results

Based on the MSK simulation procedure,[5] Fig's. 3 and 4 show the predicted dependence of the tensile ductility on the area fraction of holes for "1100 Al" and "70-30 brass" specimens of differing geometries and with different S-values or degrees of hole clustering (see Fig. 2). These predictions, which are made using only empirically represented experimental data without the use of additional parameters to force a fit, agree fairly well with experimental results from 25x125 mm^2 specimens of Al or brass; see Fig's. 3 and 4. Furthermore, Fig's. 3a and 4a show that all of these data are consistent with the normalized ductility data for porous metals[6,7] containing well-rounded porosity and with strain hardening behavior similar to the Al or brass. The reasonable agreement between the predictions of the simulations and the experimental results for both two-

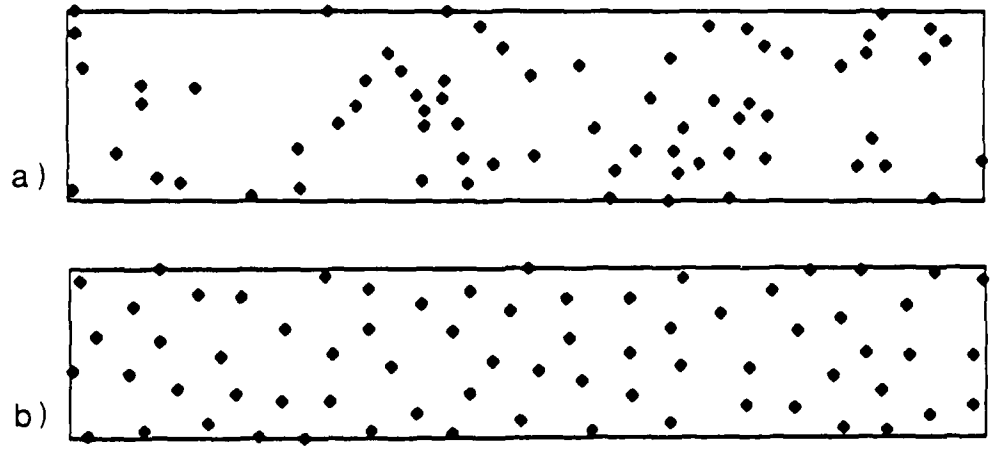

Fig. 2 Examples of random hole arrays containing 0.025 area fraction of 1.2 mm diameter holes with a length-to-width ratio of 5:1 and minimum allowable hole spacings, S, of (a) 0.5 mm and (b) 4.5 mm.

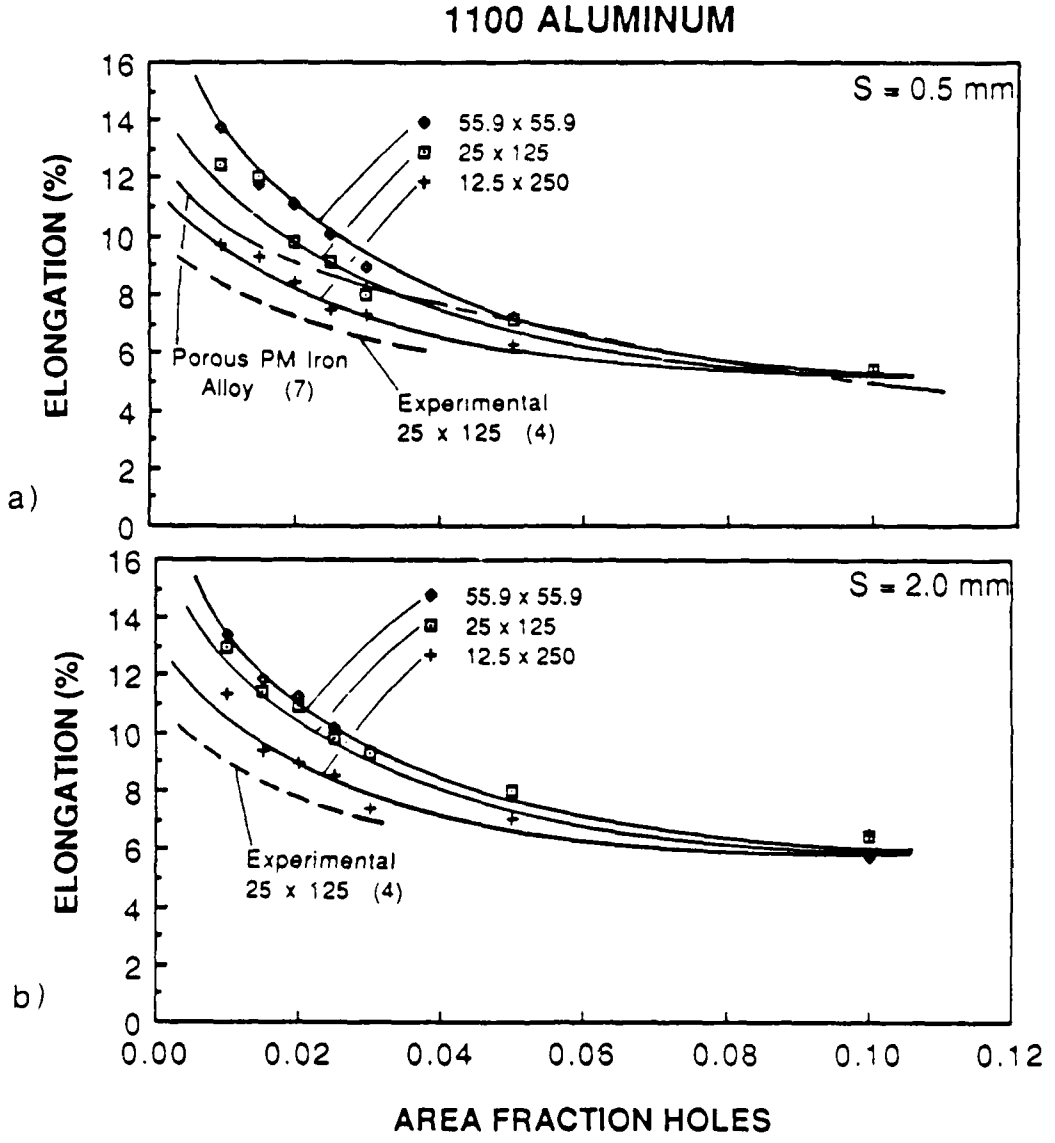

Fig. 3 The dependence of the elongation to failure on the area fraction holes for 1100 aluminum. The diameter of the holes is 2.0 mm and the minimum allowable hole spacings are (a) 0.5 mm and (b) 2.0 mm. Data from the computer simulation are shown for specimen sizes of 55.9x55.9, 25x125 and 12.5x250 mms. The curves from the experimental model shown are from ref. [4] and in (a) the curve for porous PM iron is from ref. [7].

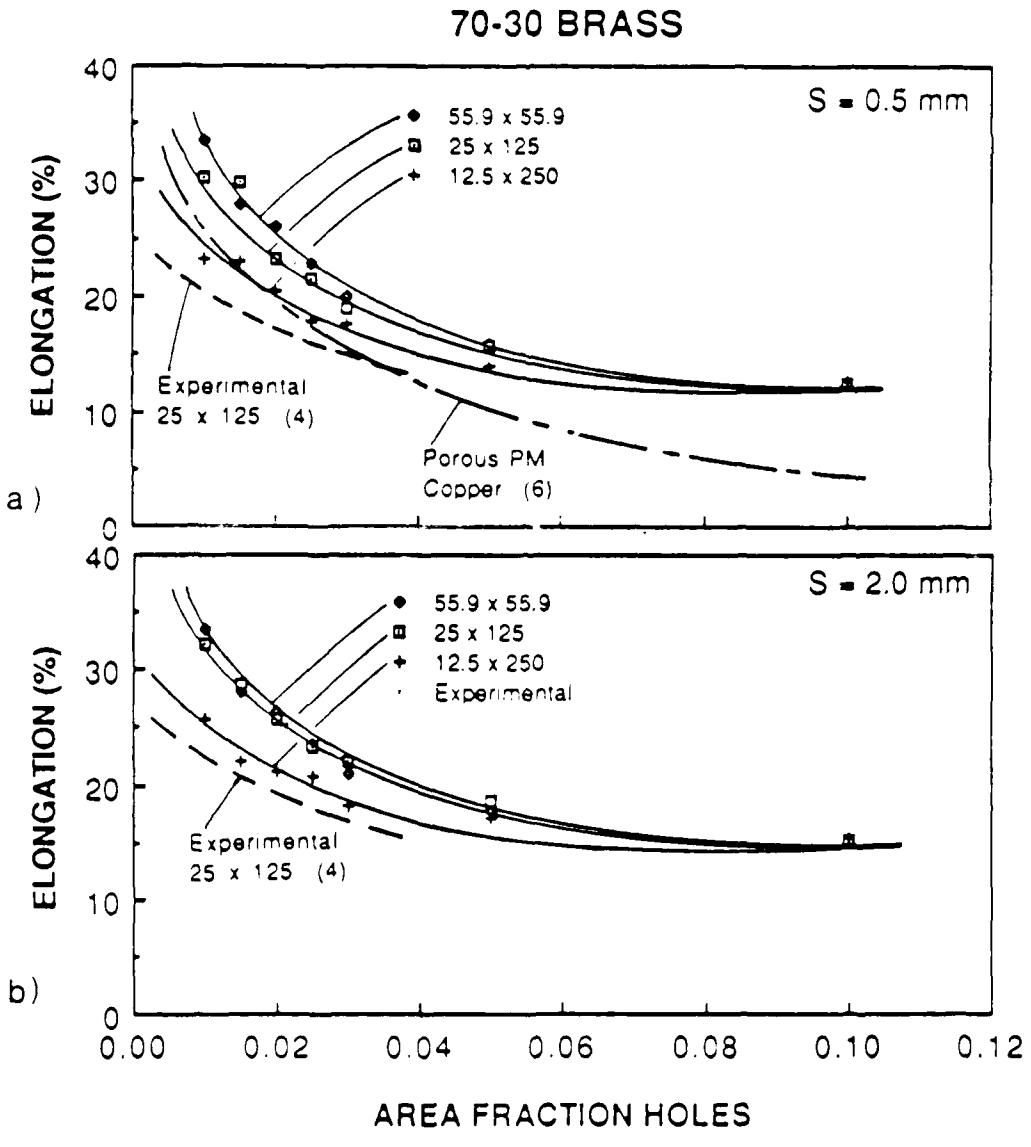

Fig. 4 The dependence of the elongation to failure on the area fraction holes for 70-30 brass. The diameter of the holes is 2.0 mm and the minimum allowable hole spacings are (a) 0.5 mm and (b) 2.0 mm. Data from the computer simulation are shown for specimen sizes of 55.9x55.9, 25x125 and 12.5x250 mms. The curves from the experimental model shown are from ref. [4] and in (a) the curve for porous PM copper is from ref. [6].

dimensional and three-dimensional materials provides strong support for the validity of this modeling scheme. Furthermore, as discussed elsewhere in detail, the simulation also correctly depicts the sequential stages of void/pore linking described earlier[3,4]. Thus we believe that the predictions of the simulation are credible.

A close examination of the simulation predictions in Fig. 3 and 4 indicate the following trends with regard to porous metals:

(1) Ductility depends on specimen shape but only at small area fractions of pores. In this case, long/narrow specimens exhibit less ductility than short/wide specimens of the same load-bearing volume.

(2) The decrease of ductility with increasing aspect ratio (length/width) of the specimen noted above is more pronounced when pores are clustered. This latter effect is illustrated by comparing Fig's. 3a and 4a (small S-values) to those of Fig. 3b and 4b (large S-values). This is also illustrated in Fig. 5 for the case of .025 area fraction of holes for an "Al" specimen.

(3) The scatter of the predicted ductility values is also significantly greater in long, narrow specimen at small area fractions of pores than at large area fractions and when pores are clustered (small S-values) than when uniformly spaced (large S-values). The degree of scatter within the ductility data can be represented through the use of Weibull statistics.[1,8] The Weibull constant m is calculated through the use of a Weibull plot, and this constant increases when the degree of scatter decreases. Fig. 6 shows the Weibull plot for the case of small and large area fractions of holes for the case when holes are clustered (S = 0.5). The Weibull constant for the small area fraction (AF = .01) is 16.2, while for the large area fraction (AF = .1), m = 9.5. Fig. 7 displays the effect of specimen geometry on the degree of scatter; clearly the ductility data have much more scatter in long, narrow specimen where m = 5.3 as compared to m = 13.5 for short, wide specimens at the same area fraction and degree of clustering. Therefore, the data shows that the statistical degree of scatter is significantly greater at small area fractions of holes/pores and in long, narrow specimens.

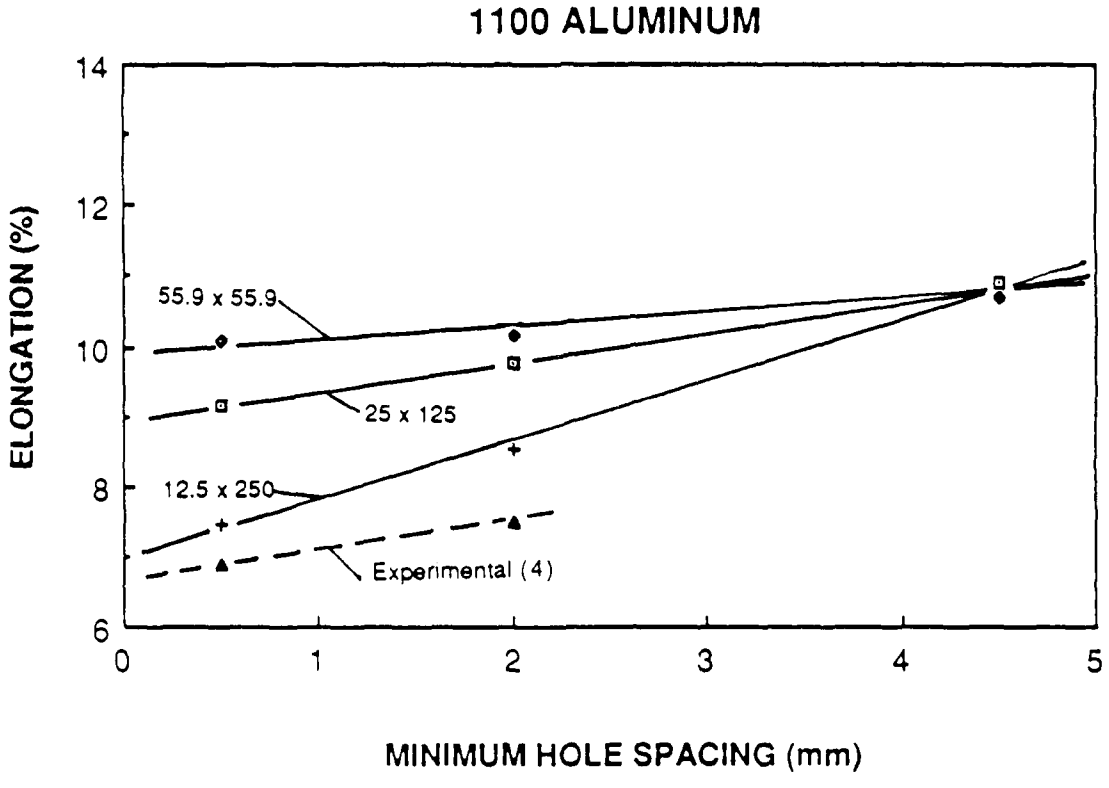

Fig. 5 The predicted dependence of the elongation to failure on the minimum allowable hole spacing for 1100 Aluminum containing 0.025 area fraction of 2.0 mm diameter holes as a function of specimen shape. Data from the experimental model is from ref. [4].

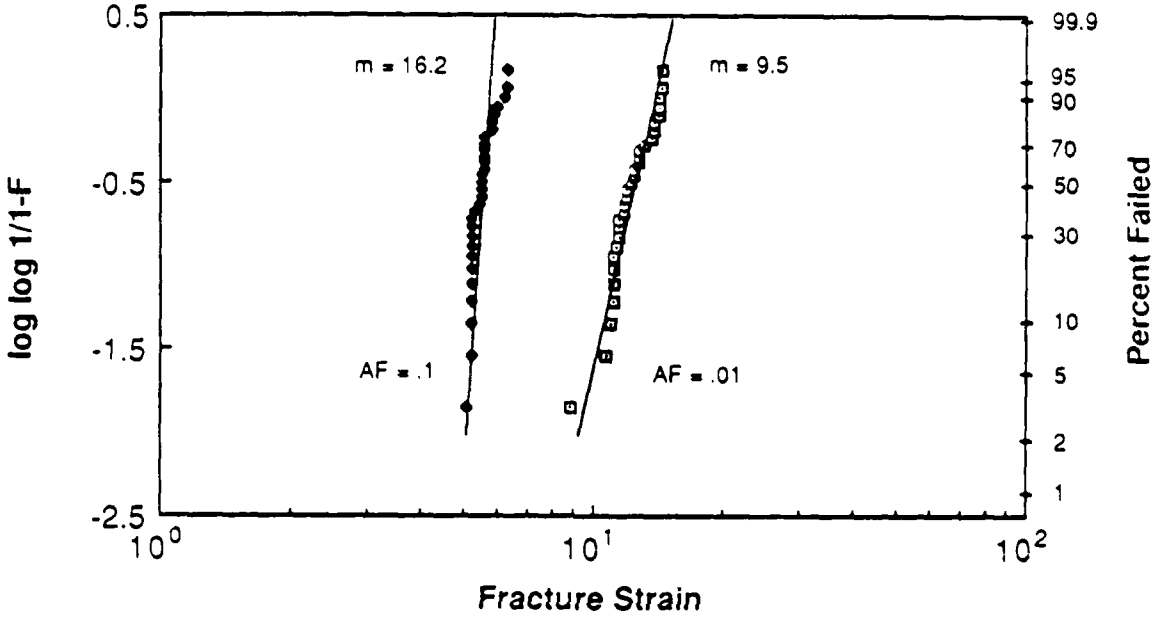

Fig. 6 Weibull plots predicted ductilities of 1100 aluminum specimens containing 0.1 and 0.01 area fraction of 2.0 mm diameter holes with a minimum allowable hole spacing of 0.5 mm and a specimen size of 25x125 mm. The Weibull constant m is shown for each case.

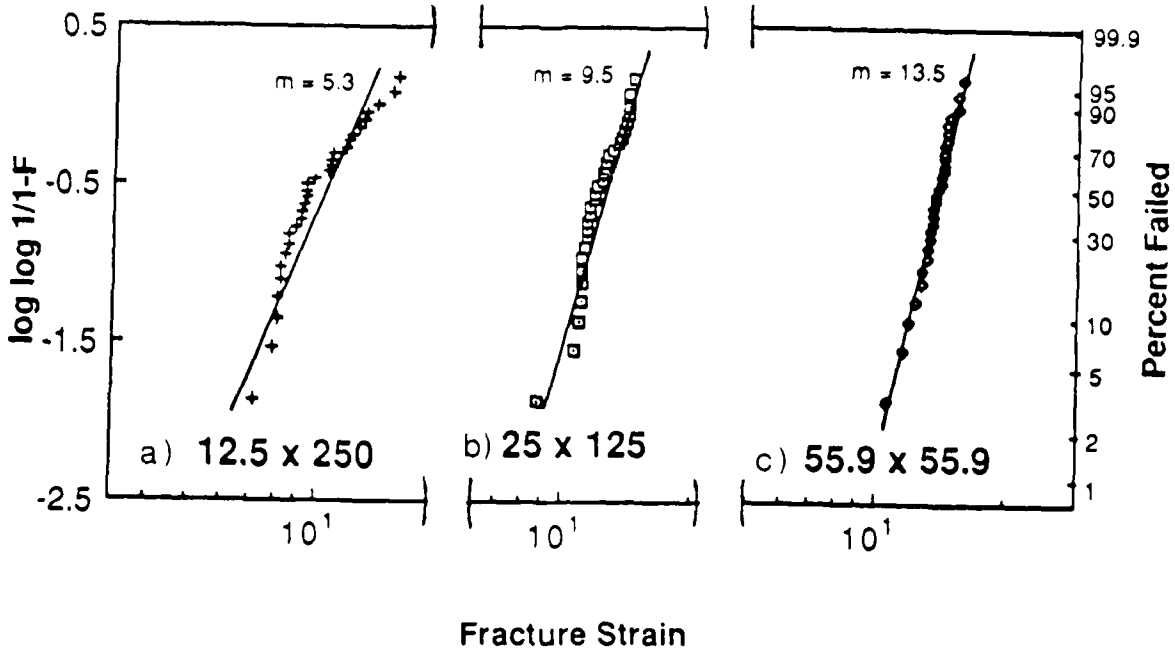

Fig. 7 Weibull plots for 1100 aluminum specimens containing 0.01 area fraction of 2.0 mm diameter holes with a minimum allowable hole spacing of 0.5 mm and a specimen size of (a) 12.5x250, (b) 25x125 and (c) 55.9x55.9 mm.

In summary, the simulations predict that long, narrow specimens with high aspect ratios should exhibit a loss of ductility which is most pronounced (a) at low area fractions of pores, and (b) when pore distributions exhibit a high degree of clustering. Furthermore, in such cases there will also be a high degree of scatter in the ductility data; i.e. the material exhibits a comparatively low Weibull modulus for a metal fracture process.

C. An Analysis of the Specimen Shape Effects and "Imperfections" in Porous Metals.

1. Background: Imperfections in Deforming Porous Metals

The above results are fully consistent with qualitative basis of imperfection theory as originally formulated for the localized necking of sheet metal by Marciniak and Kucyznski.[9] There have been several extensions of that analysis, notably to fracture in general [10-12] and fracture of voided materials in particular[13]. Imperfection analysis typically assumes a pre-existing imperfection or "band of weakness" which extends across the load bearing cross section of a strip or specimen undergoing plastic deformation. The imperfection may be a physical groove, a band of weak material or, in our case, a band of material which contains a higher area fraction of pores. Normally in such an analysis, the severity of the imperfection is fixed at an initial value which, in our case, would be characteristic of the starting pore microstructure. For example, consider that the band of material labeled B in Fig. 8a contains a higher pore volume fraction than the adjacent material A. As shown in Fig. 8b, transfer of load along the specimen length dictates that the strain in B exceeds that in A, since the load in B equals that in A. Thus, as the specimen deforms in this plane strain example, flow localization occurs within the B strip at a macroscopic limit strain ε_A^*; see Fig. 8c.

While depending on both strain and strain-rate hardening, ε_A^* is also a very sensitive function of the severity of the imperfection. Specifically, if an imperfection or inhomogeneity factor, f, has the value of unity in a perfectly homogeneous or uniform

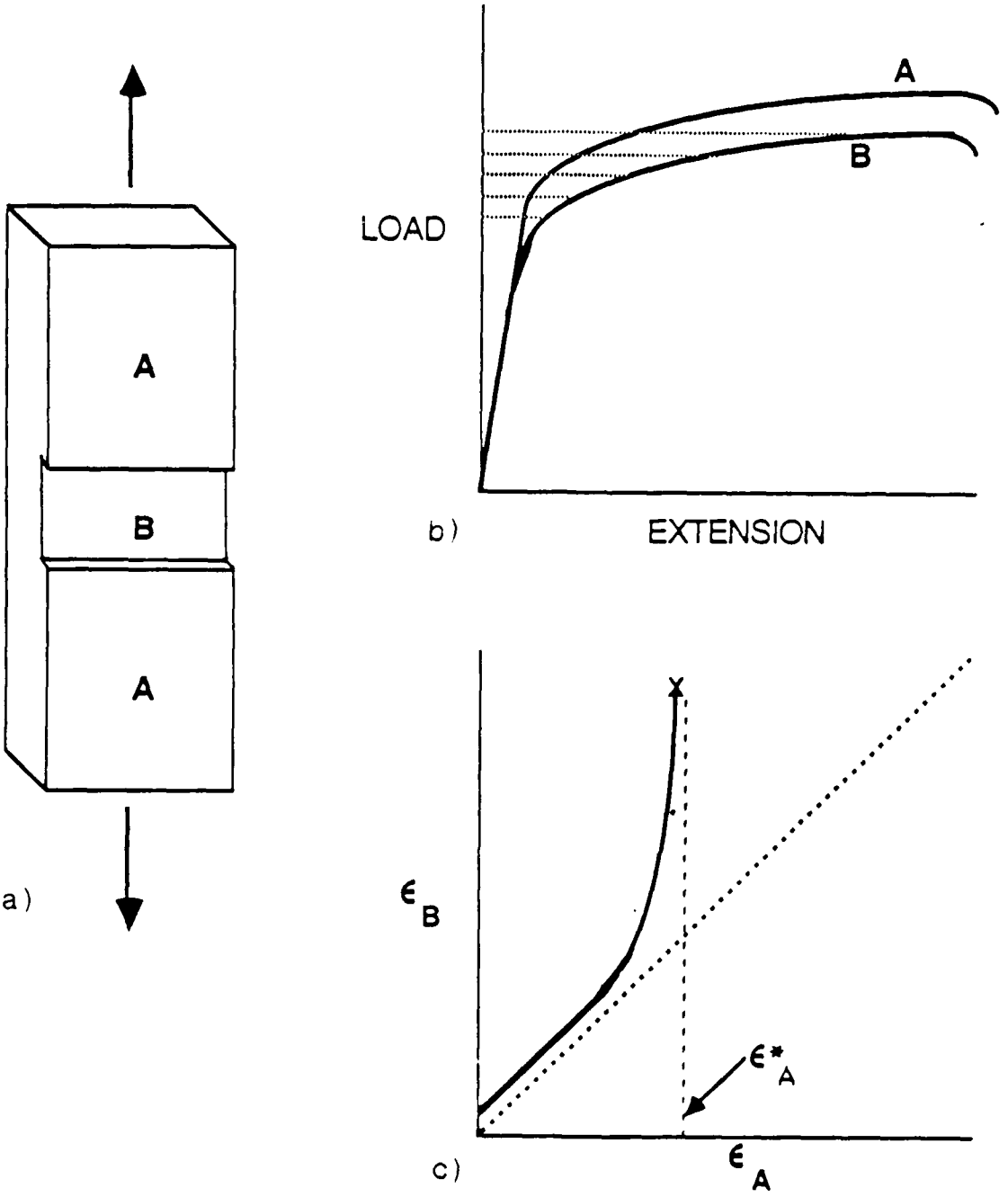

Fig. 8 A schematic depicting the basis for imperfection theory. (a) A free-body diagram of a sample with an imperfection or band of weak material labelled B. (b) A representation of the load versus extension curves for the two bands of material shown in (a). (c) Example of flow localization in the band of weak material and the macroscopic limit strain, ε^*_A.

material, then it may be defined such that its value decreases as the severity of the imperfection increases. In the present case of randomly located pores along the specimen length, f may be taken as $f = A(x)/A_o$, where A(x) is the porosity-reduced load-bearing cross section area at a position X along the specimen length as compared to A_o which is the maximum load-bearing cross section area along the entire gauge length.+ The initial value of f has a strong influence on ε^*_A. For example, increasing the severity of a single imperfection by decreasing the f-value from 0.99 to 0.97 will decrease ε^* from 1.0 to 0.6 in the uniaxial tension of a material with n = 0.20 containing an imperfection normal to the maximum principal strain axis[14].

We propose that in a ductile material containing porosity that there are (a) initial imperfections along the specimen length due to the pore distribution (denoted by f_o) as well as (b) "linking-induced" imperfections which are created as the linking of pores removes load-bearing ligaments during straining and which are denoted f_1. These two types of imperfections are shown schematically in Fig. 9. It should be noted that the eventual dominant imperfection failure after strain-induced hole linking occurs at a position which may not have the lowest initial value. Rather the eventual dominant imperfection contains a group of pores which, due to their close spacing, also link easily during deformation, creating a severe imperfection, which corresponds to a small f_1-value. As a result, specimen failure occurs due to the associated flow localization process which causes fractures on a zig-zag plane of high pore content (typically about 8 times random)[13] with microvoid coalescence occurring within the ligaments between the pores at very high local strains.

The characteristics of the initial and subsequent linking-induced imperfection factors may now be examined. Recalling that $f = A(x)/A_o$ and applying a uniform load P along the length of the specimen, the initial imperfection factor f_o is

---

+ Barring stress concentration effects, the value of A_o would be $A_o = A(1-V_f)$ where A is the total cross section area and V_f is the minimum value of the volume fraction of porosity within any given strip of material along the gauge length.

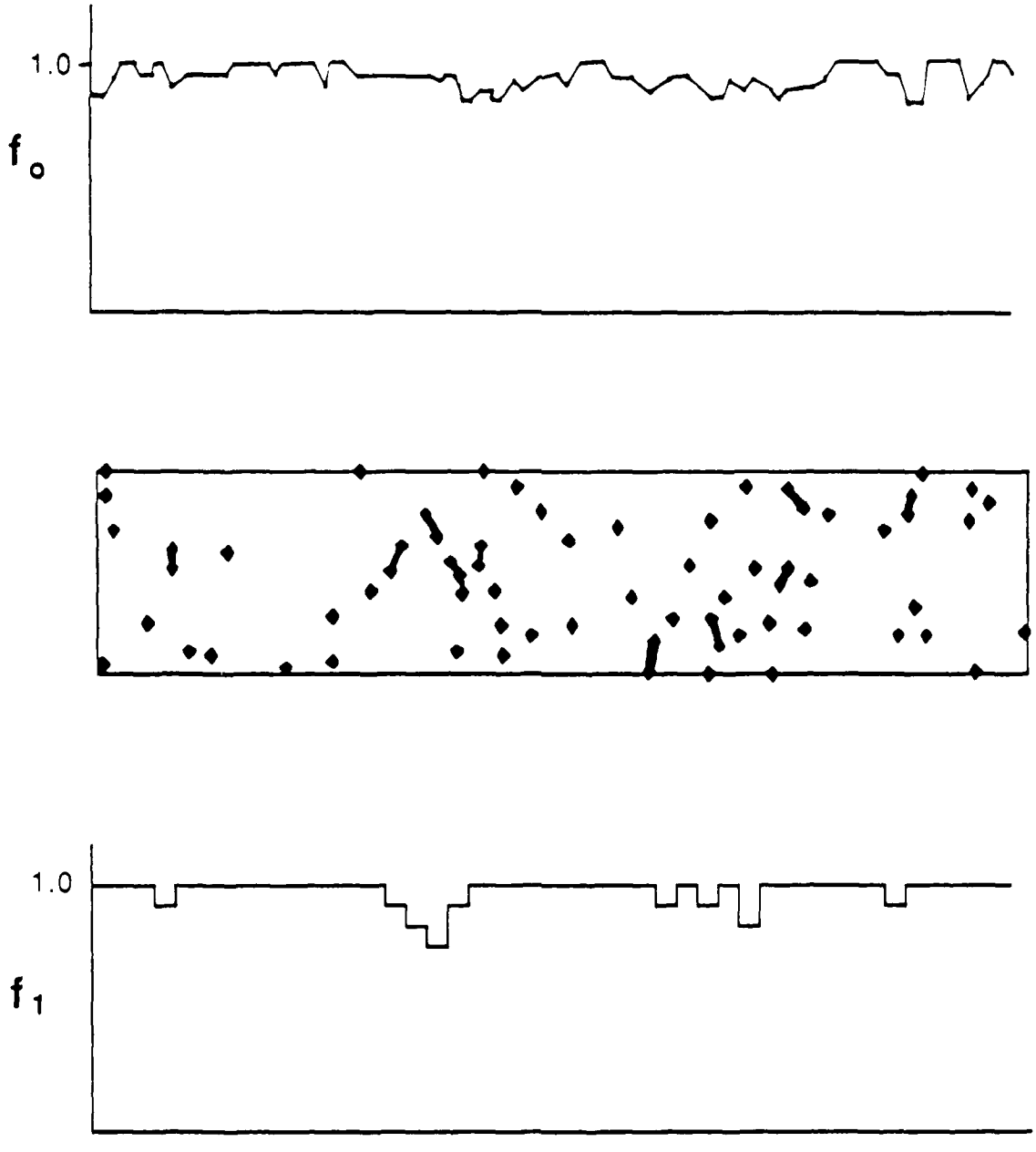

Fig. 9 A schematic of the initial imperfection factor f_o and linking-induced imperfection factor f_1 for the specimen shown with selected linked holes.

$$f_o(x) = A(x)/A_o = \sigma_o/\sigma(x), \quad (1)$$

where σ_o is the section stress within the matrix material with the maximum load-bearing cross section and $\sigma(x)$ is the section stress within a band of matrix material located at position X along specimen length. Fig. 9a illustrates the dependence of f_o on pore distribution. At a strain after which pore linking has occurred but before specimen failure, the loss of load-bearing capacity of failed ligaments between pores within the specimen will create a linking-induced imperfection factor f_l which depends on both strain ε and position x:

$$f_l(\varepsilon,x) = \sigma_o'/\sigma' \quad (2)$$

In Eq. 2, σ_o' is the section stress that would occur within the specimen assuming that there are no pores present while σ' is the section stress at position x after N ligaments have failed within that band during straining. In most cases, $\sigma_o' \simeq \sigma_o$. If each failed ligament has an average load-bearing, cross-section area A_l, then

$$f_l(\varepsilon,x) = \frac{P/A}{P/(A-NA_l)} = 1 - \frac{NA_l}{A} \quad (3)$$

where A is the cross-sectional area of the load-bearing matrix material in the absence of holes . It should be noted that Eq. 3 implicitly ignores any localized stress concentrations which may have been caused by pore linking. The strain dependence of $f_l(\varepsilon,x)$ is caused by the dependence of pore linking on strain; thus $N = N(\varepsilon,x)$.

The total imperfection factor f_T within any band of material across the specimen reflects the combined effects of the initial pore distribution (Eq. 1) and the linking-induced effects (Eq. 3) such that

$$f_T(\varepsilon,x) = f_o f_l = \frac{\sigma_o}{\sigma(x)}\left[1 - \frac{NA_l}{A}\right] \quad (4)$$

Eq. (4) indicates that a severe imperfection (small value of $f_T(\epsilon,x)$) occurs along the specimen or component length when (a) there is a pre-existing cluster of pores within a strip at x which significantly increases that section stress $\sigma(x)$, (b) a large number, N, of closely spaced pores link within a strip of load-bearing material during specimen straining, (c) pores spaced far apart (large A_l-values) link (perhaps due to irregularly shaped pores whose long axis is normal to the maximum principal strain axis), and (d) of special interest to the present study, the value of A is small (small cross sectional area of the specimen).

2. Analysis of Specimen Shape Effects

The specimen shape effects previously described may now be analyzed in terms of the imperfection analysis above. The observed trends may be understood as follows:

a) Ductility depends on specimen shape but only at small area fractions of pores. In this case, long/narrow specimens exhibit less ductility than short/wide specimens.

Eq. 4 indicates that $f_T(x,\epsilon)$ is severe and has a small value when ratio of NA_l/A is large. This occurs when the effective cross section area A of the specimen is small and a large degree of linking occurs which corresponds to large NA_l values. The result causes a severe linking-induced imperfection. In Eq. 4, the initial imperfection factor $\sigma_o/\sigma(x)$ will be also sensitive to specimen shape effects, increasing in severity in long, narrow specimens. For example, a same cluster of pores will increase $\sigma(x)$ much more if that stress is based on a small cross section area, rather than a large one. Similar rationale applies to the effect of area fraction of pores; specifically that the specimen geometry effects are manifested only at small area fractions of pores. In this case, it is important to recognize that the imperfection relates to the bands of materials across the specimen width which contain a higher density of initial and/or linked pores than neighboring bands. This effect is

most likely to occur at low area fractions of pores since even small differences in initial pore/linked pore density will be significant in such a case.

b) The decrease in ductility with increasing specimen aspect ratio is more pronounced when pores are clustered.

The clustering of pores affects the initial imperfection factor f_0 by creating strips of high pore content (see Fig. 9). Clustering also causes pore linking, thus causing f_1 to decrease rapidly with strain at certain positions X along the specimen length. Thus in Eq. 4 both f_0 and f_1 are sensitive to clustering.

c) The scatter of predicted ductility values is greater at when pores are clustered at small area fractions of pores, and in long, narrow specimens.

This effect relates to the likelihood of a single severe imperfection quickly dominating deformation and causing failure at small strains. For this to occur, a significant non-uniformity of pore population must occur across the specimen width. This situation is most likely to occur at small area fractions of pores, when pores are clustered, and in specimens of high aspect ratio.

3. Implications to Porosity and Fracture Toughness.

The specimen shape and imperfection considerations discussed above contain implications to the effects of porosity on fracture toughness. Specifically, it is frequently the case that porosity affects tensile ductility much more adversely than fracture toughness.[15,16] This effect may be understood in terms of the imperfection analysis. Specifically, at the onset of rapid crack growth, fracture occurs within a very small volume of material constrained to the location immediately ahead of a relative flat, planar crack front. In contrast, a very large volume of material is subjected to deformation in a tensile test. Thus,

the deforming tensile specimen fails along paths conciding with severe imperfections consisting of clustered, linked pores on planes of high pore content. in contrast, initial crack growth must occur via pore linking along a relatively pre-determined path, which concides with planes of high pore content. Thus, the volume of material sampled for pore-induced imperfections is quite small in a fracture toughness experiment and initial crack growth, which determines the fracture toughness parameter, occurs through comparatively "perfect" material.

SUMMARY

The present analysis indicates that porosity decreases ductility to a greater extent in long, narrow specimen than in short, wide ones. Furthermore, the effect is likely to be significant only at small volume fractions of porosity and when pores are clustered. Under these conditions, there will also be a comparatively large scatter in ductility values from specimen to specimen. These effects can be readily understood in terms of imperfection theory, which also provides a basis for understanding the fact that porosity usually influences tensile ductility much more than fracture toughness.

ACKNOWLEDGEMENTS

The authors are grateful to Dr's. P. Magnusen and D. Srolovitz for helpful comments. This research was supported by the Office of Naval Research through Contract No. N00014-86-K-0381.

REFERENCES

1. R. W. Davidge, Mechanical Behavior of Ceramics, (Cambridge University Press, Cambridge) 1986, p. 133.
2. N.E. Frost, K.J. March, L.P. Pook, Metal Fatigue, (Clarendon Press, Oxford) 1974, p. 54.
3. E.M. Dubensky and D.A. Koss, Metall. Trans A, 18A , 1887 (1987)
4. P.E. Magnusen, E.M. Dubensky and D.A. Koss, Acta Metal 36, 1503 (1988)
5. P.E. Magnusen, D.J. Srolovitz and D.A. Koss, Int. J. Fracture (to be published).
6. B.I. Edelson and W.M. Baldwin, Trans. Am. Soc. Metals 55, 230 (1962)
7. K. M. Vedula and R. W. Heckel, Modern Developments in Powder Metallurgy, Vol. 12 eds. H. H. Hausner, H. W. Antes and G. D. Smith, MPIF, 1981.
8. W. Weibull, J. Appl. Mech. 18, 293 (1951).
9. Z. Marciniak and K. Kuczynski, Int. J. Mech. Sci 9, 609 (1967)
10. Z. Marciniak and K. Kuczynski, Int. J. Mech. Sci 21, 609 (1979)
11. H. Yamamoto, Int. J. Fract. 14, 347 (1987)
12. M. Saje, J. Pan and A. Needleman, Int. J. Fract. 19, 163 (1982)
13. R.J. Bourcier, D.A. Koss, R.E. Smelser and O. Richmond, Acta. Met. 34, 2443 (1986)
14. K.S. Chan and D.A. Koss, unpublished research
15. J. T. Barnby, D. C. Ghosh and K. Dinsdale, Powder Met., 16, 55, (1973).
16. N.R. Moody, W.M. Garrison and J.E. Swiggeresky, unpublished research